Characterization and Application of Nanomaterials (2021) Volume 4 Issue 2
doi:10.24294/can.v4i2.1336

ORIGINAL RESEARCH ARTICLE

Spin thermoelectric effects on aluminum or phosphorus doped zigzag silicene nanoribbons

Jiali Song[1], Xue Zhang[1], Xuefeng Wang[2], Jinfu Feng[1,3], Yushen Liu[1,3*]

[1] *School of Physics and Electronic Engineering, Changshu Institute of Technology, Changshu 215500, China*

[2] *Jiangsu Laboratory of Advanced Functional Materials, Changshu 215500, China*

[3] *School of Physical Science and Technology, Soochow University, Suzhou 215006, China. E-mail: ysliu@cslg.cn*

ABSTRACT

Based on the density-functional theory (DFT) combined with nonequilibrium Green's function (NGF), this paper investigates the effects of either single aluminum (Al) or single phosphorus (P) atom substitutions at different edge positions of zigzag-edged silicene nanoribbons (ZGNRs) in the ferromagnetic state on the spin-dependent transport properties and spin thermoelectric effects. It has been found that the spin polarization at the Fermi level can reach 100% or –100% in the doped ZSiNRs. Meanwhile, the spin-up Seebeck effect (for –100% case) and spin-down Seebeck effect (for 100% case) are also enhanced. Moreover, the spin Seebeck coefficient is much larger than the corresponding charge Seebeck coefficient at a special doping position and electron energy. Therefore, the study shows that the Al or P doped ZSiNRs can be used to prepare the ideal thermospin devices.

Keywords: Silicene Nanoribbons; Doping; Spin Seebeck Coefficients

ARTICLE INFO

Received: 10 August 2021
Accepted: 4 October 2021
Available online: 9 October 2021

1. Introduction

Since graphene was successfully prepared by mechanical method for the first time in 2004, people have become more and more interested in other two-dimensional honeycomb structural materials[1]. Among them, silicone material is such a structure-silicon atoms of two-dimensional hexagonal lattice. Unlike graphene with planar structure, because the distance between silicon atoms is farther than that between carbon atoms, therefore, silene has a low degree of fold structure, and the distance between its two silicon atoms is about 0.44 Å[2]. Its unique geometry brings many interesting properties, such as quantum Hall effect[3], large spin orbit interaction[4] and mechanically adjustable energy gap[5]. Similar to graphene, in the Fermi level and zero band gap structure, silene has a semi metallic low energy state. Although spin orbit coupling can open an energy gap at the Dirac energy point, its value is only 1.5 meV[3]. However, from the perspective of application, we need to open a relatively large energy gap. Silene nanoribbons provide a feasible method. Recent experimental studies have confirmed that one-dimensional silene nanostructures can be prepared[6]. Similar to graphene ribbons, silene nanoribbons also have two types of edges, namely serrated silene ribbons (ZSiNRs) and armrest silene ribbons (ASiNRs). Hydrogen saturated armrest nano ribbons can behave as semiconductors and metals according to the change of their length. However, the

ground state of hydrogen saturated sawtooth silene nano ribbons is the boundary antiferromagnetically coupled semiconductor state[6]. Under the action of the transverse electric field, for boundary doping with phosphorus or nitrogen atoms in the serrated silene nanoband, its magnetic semiconductor state can be converted into a semimetallic state[7].

Recently, molecular dynamics studies have shown that the boundary hydrogen saturated silene nanoribbons have very good stability, and their geometry even exists under 800 K temperature[8]. This shows that hydrogen saturated silene nanoribbons can be used to prepare very stable thermoelectric devices. Based on the first principle method, Zberecki *et al.* found that due to a conductivity gap on the Fermi surface, its conductivity is extremely suppressed. Due to the inverse relationship between Seebeck coefficient and conductivity in the low temperature region, it leads to the great increase of its thermoelectric coefficient[9]. In addition, with the maturity of spin detection technology, people can detect spin current through spin Hall effect. In 2008, the phenomenon that a spin flow can arise when a temperature gradient is applied at both ends of the magnetic metal Ni81Fe19 connected to the Pt line was found by Uchida et al[10]. Similar to the traditional charge thermoelectric effect, this effect is called "spin Seebeck effect" or "thermal spin effect". This pioneering experiment has stimulated a large number of relevant theoretical and experimental studies[11–17]. When the silene nanoribbons are in the boundary ferromagnetic coupling state, they exhibit spin degenerate metal behavior at the Fermi plane. Because the boundary antiferromagnetic state shows semiconductor behavior, such a large magnetoresistance behavior can be found[18].

In this paper, the spin thermoelectric effect of single aluminum (Al) or phosphorus (P) atomic boundary instead of doped ZSiNRs double probe structure will be studied in the first principle (see **Figure 1**). This device consists of the left electrode part, the intermediate scattering region, and the right electrode part. The width of ZSiNRs is 6. We consider four different boundary doping positions and find that for Al atom doping, the spin polarization at the Fermi plane is close to –100% at the second and third positions, but it is just the opposite for P atom doping. The results show that for phosphorus atom doping, at position 3, the spin polarizability at the Fermi surface reaches 100%. The main reason is that there are transmission nodes at the Fermi surface. At the same time, the spin thermoelectric coefficient at the Fermi is also significantly strengthened By adjusting the electron energy, the spin thermoelectric coefficient of doped ZSiNRs can be similar to or even greater than the charge thermoelectric coefficient.

2. Model establishment

Bilateral monohydrogenated ZSiNRs are used as the original package of the nano system, and the bandwidth is generally taken as 6. Using VASP software package, we first optimized the FM state single package structure of hydrogenated ZSiNRs, and the cut-off energy is taken as 360 eV[19]. The exchange correlation function adopts generalized gradient approximation (GGAPBE). The maximum force per atom does not exceed 0.01 eVA^{-1}. After geometric optimization, based on the original package structure, this paper designed a nano double probe system as shown in **Figure 1**. The boundary Si atoms are saturated with H atoms. The Si atoms with middle marks 1–4 in the middle scattering region are replaced with other atoms respectively (i.e. only one Si atom is replaced for each doping). The atoms replaced in this paper include Al and P. Here, for simplicity, Al doped silene nanoribbons are referred to as Al-ZSiNRs; P-doped silene nanoribbons are abbreviated as P-ZSiNRs.

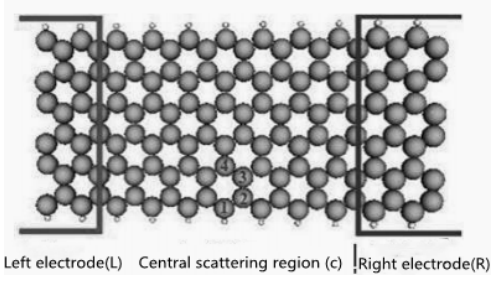

Figure 1. A spin device structure composed of 6-ZSiNRs. The box on the left represents the left electrode and the box on the right represents the right electrode. 1–4 in the figure represents different doping positions in the scattering region. The large ball represents Si atom and the small ball represents H atom.

In this paper, a software package Atomistix Toolkit (ATK) based on nonequilibrium Green's function and density functional theory is used to complete the calculation and Simulation of the electron transport process of the system. The system optimization adopts Newton optimization. The exchange correlation function adopts generalized gradient approximation (GGA), and the basis vector adopts DZP (Double Zeta Polarized). The size of the contracted Brillouin area is set to (1, 1, 100). In order to avoid the interaction between images, the vacuum layer is taken as 15 Å and the energy truncation radius is taken as 150 Ry.

The electron transmission coefficient of the eigenenergy of E is:

$$\tau_\sigma(E) = T_r[\,\Gamma_L(E)\,G^r(E)\,\Gamma_R(E)\,G^a(E)\,]_\sigma \quad (1)$$

Here $\Gamma_{L/R}(E)$ is the wire width function of the central center coupled to the left/right wire, σ is the spin exponential index and E is the energy. $G_{R/A}(E)$ is the delayed and advance Green function of the central scattering region and can be calculated by equations $G_\sigma^r = [E\mathrm{I} - H + i(\Gamma_{L\sigma} + \Gamma_{R\sigma})/2]^{-1}$ and $G_\sigma^a = [Gr_\sigma^r]$. I is the unit matrix and H is the Hamiltonian of the central scattering region.

The spin polarizability at the Fermi plane can be defined as:

$$P = \frac{\tau_\uparrow - \tau_\downarrow}{\tau_\uparrow + \tau_\downarrow} \times 100\% \quad (2)$$

In order to study the spin thermoelectric effect, we give the expression of spin dependent Seebeck coefficient in the linear region:

$$S_\sigma = -\frac{L_{1\sigma}(\mu, T)}{|e|TL_{0\sigma}(\mu, T)} \quad (3)$$

Where,

$L_n = \sum_\sigma L_{n\sigma}$, $L_{n\sigma} = -\frac{1}{h}\int dE T_\sigma(E)(E-\mu)^n \frac{\partial f}{\partial E}, n = 0,1,2$, $f_{L(R)}$ is the Fermi Dirac distribution function. Spin Seebeck coefficient is expressed as $S_s = (S_\uparrow - S_\downarrow)/2$, and the corresponding charge Seebeck coefficient is $S_c = (S_\uparrow + S_\downarrow)/2$[20].

3. Results and discussion

Formula (3) can be reduced at low temperatures to:

$$S_\sigma(\mu) \simeq -\frac{\pi^2 k_B^2 T}{3e}\frac{\tau_0'}{\tau_0}(\mu) \quad (4)$$

The formula (4) shows that the spin-dependent Seebeck coefficient and transmission odds are proportional to the slope of the energy, and inversely proportional to its size. **Figure 2(a)** shows the transmission spectrum of pure ZSiNRs in the energy range [–2 eV, 2 eV]. It can be seen from **Figure 2(a)** that the complete ZSiNRs shows typical metal behavior, that is, the transmission function value near the Fermi level ($E = E_F = 0$), $\tau_\sigma(E) = 1$ is a constant. The upper and lower spin channels are almost degenerate. For the spin-up channel, a peak is generated in the energy $E - E_F \approx -0.2$ eV region, and its transmission function value is $\tau_\sigma(E) \approx 3$. For the spin-down channel, a peak is generated near the energy $E - E_F \approx 0.1$ eV, and its transmission function value is $\tau_\sigma(E) \approx 3$. **Figure 2(b)** shows the relationship between the spin-dependent thermoelectric coefficient S_σ and the chemical potential μ for the pure ZSiNRs. Here the

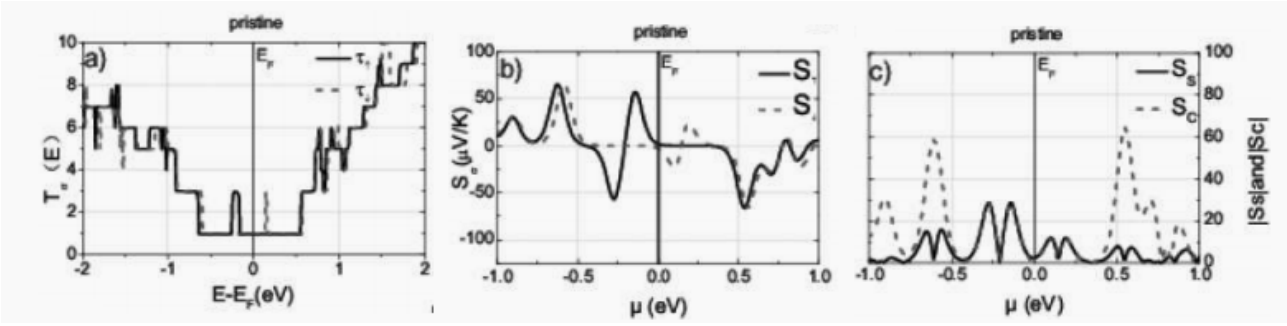

Figure 2. The transmission spectrum and thermal power coefficients of the full ZSiNRs at zero bias. **(a)** For the T_0-energy relation diagram, **(b)** and **(c)** for the absolute value of the spin-correlation thermoelectric coefficient Sσ and the spin (charge) Seebeck coefficient for the pure ZSiNRs $|S_S|(|S_C|)$.

temperature is taken as 300 K. We find that with the change of chemical potential μ, the spin-associated thermoelectric coefficient S_σ of the full ZSiNRs (FM state) is significantly enhanced at the position where the transport function has mutations. The spin polarizability at the Fermi surface is close to zero and its Seebeck coefficient is very weak. The main reason is that the slope of the transmission probability at the Fermi surface is almost zero.

Figure 3 shows the spin dependent transmission spectra of ZSiNRs with different doping types and doping positions. From the figure, we can see that when ZSiNRs is doped, the upper and lower spin electron transport characteristics appear non-degenerate phenomenon, and the non-degenerate phenomenon shows different behavior with different doping positions (position 1 turns to 4 in turn). There are some conductivity troughs on both sides of Fermi level (also known as local quantum state). The transmission spectrum of doped ZSiNRs is related not only to the spin direction, but also to the type and position of doping. As shown in **Figures 3(a)** and **(b)**, when the edge of pure ZSiNRs along Si atom (**Figure 1**, position 1) is replaced by Al or P atoms, the metal behavior near the Fermi level remains almost unchanged, and the spin degeneracy phenomenon is still obvious. For spin-up electrons both doping causes a conductance trough at energy slightly below E_F and for spin-down electrons a similar narrow decrease at energy slightly above E_F, there was a more pronounced decrease near the $|E - E_F| \approx 0.5$ eV, with a decrease in the transmission function of both the upper and lower spins. When the doping position is moved to position 2 in **Figure 1**, the transmission spectrum of Al-ZSiNRs in **Figure 3(c)** changes more obviously, and its spin degeneracy is destroyed. At the Fermi level ($E - E_F = 0$), the upper spin transmission function of Al doped ZSiNRs is obviously suppressed, while the lower spin transmission function remains unchanged. **Figure 3(d)** shows that the transmission function of P-ZSiNRs is just the opposite here. Compared with the change of the transmission spectrum of doped ZSiNRs at position 1, the spin dependent local quantum state of P-ZSiNRs near $E - E_F \approx -0.5$ eV disappears; while the spin dependent local quantum state of Al-ZSiNRs near $E - E_F \approx 0.5$ eV disappears, and there are more narrow falling states near $E - E_F \approx -0.5$ Ev. When the doping position moves to position 3, the spin degeneracy of the transmission spectra of Al-ZSiNRs or P-ZSiNRs in **Figures 3(e)** and **(f)** is further destroyed, and the former is more obvious. Interestingly, at the Fermi level ($E - E_F = 0$) nearby, the inhibition of the upper-spin transmission function of Al-ZSiNRs intensifies, $\tau_\uparrow = 0$, that is, the spin upward behavior of ZSiNRs changes from metallicity to insulation, while the lower-spin transmission function remains unchanged; its spin polarizability even reaches –100%. The case of P-ZSiNRs transmission function is just the opposite. Its spin polarizability can be close to 100%. Similarly, the transmission function of Al-ZSiNRs at $E - E_F \approx 0.5$ eV also has a trough, while the trough of P-ZSiNRs appears at $E - E_F \approx 0.5$ eV. When the doping is further to position 4, for the two spin channels, the transmission function of doped ZSiNRs shows cash properties near the Fermi level, and the metal behavior of the system is restored.

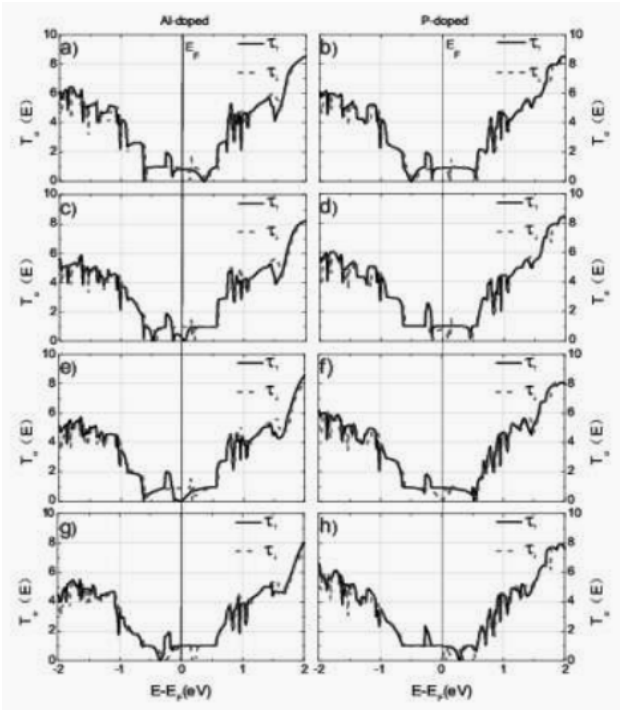

Figure 3. Transmission spectrum of the ferromagnetic state ZSiNRs doped with Al (left) and P (right) at zero bias. Black and red lines are represented, upper spin and lower spin electrons, respectively. The left and right columns represent the ZSiNRs transmission spectra at different doping positions of Al and P, respectively.

Figure 4 and **Figure 5** show the relationship between the spin-dependent thermoelectric coefficient S_σ and the spin (charge) Seebeck coefficient $S_s(S_c)$ and the chemical potential μ of the ZSiNRs for different doping positions and types, respectively. Here, the temperature T = 300 K. For each spin channel of the pure silene band, the transmission spectrum is spin-degenerate. Since $\tau_{E=E_F} = 1$ and $\tau'(E_F) = 0$, $S_\sigma = 0$, near the transmission probability node, the corresponding spin thermoelectric effect is significantly strengthened. For example, when the doping position is 1, both the spin-dependent thermoelectric coefficient S_σ of **Figure 4(a)** at $\mu \approx 0.2$ eV and (b) P-ZSiNRs at $\mu \approx -0.5$ eV, ZSiNRs is enhanced. Only the positions of the positive maximum and negative maximum of $S_\uparrow$ and $S_\downarrow$ are slightly different, which leads to the obvious strengthening of the spin thermoelectric effect, which is comparable to the corresponding charges (as shown in **Figures 5(a)** and **(b)**). However, the thermoelectric effect at the Fermi plane is relatively weak. With the doping position moving to position 2, the $S_\uparrow$ corresponding to the μ = 0 of Al-ZSiNRs is significantly strengthened, but $S_\downarrow$ maintains a relatively weak value. The main reason is that there is a node in the spin upward transmission probability at about 0.05 eV on the Fermi plane. Since the slope of $\tau_\uparrow$ at the Fermi plane is positive, according to the formula (4), its value should be negative, which is in good agreement with our numerical results (as shown in **Figure 4(c)**). While **4(d)** P-ZSiNRs shows that the spin dependent thermoelectric effect is relatively weak at $\mu = 0$.

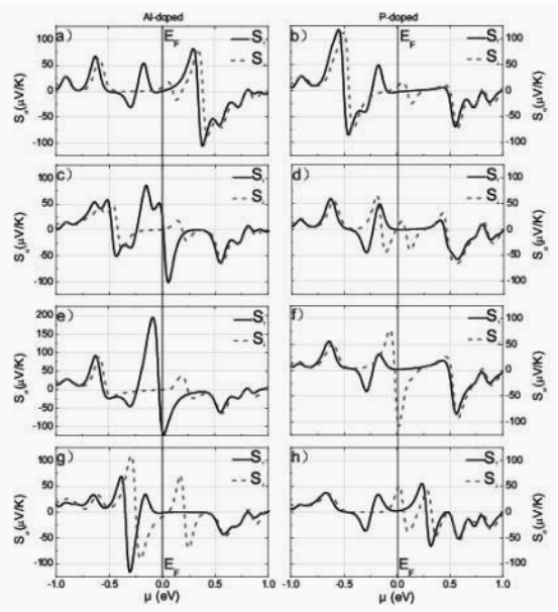

Figure 4. Spin-dependent thermoelectric coefficient function Sσ of chemical potential μ for the ferro ZSiNRs of Al (left) and P (right) at zero bias. Black and red lines represent upper spin and lower spin electrons, respectively. The left and right columns represent ZSiNRs at different doping positions of Al (left) and P (right), respectively.

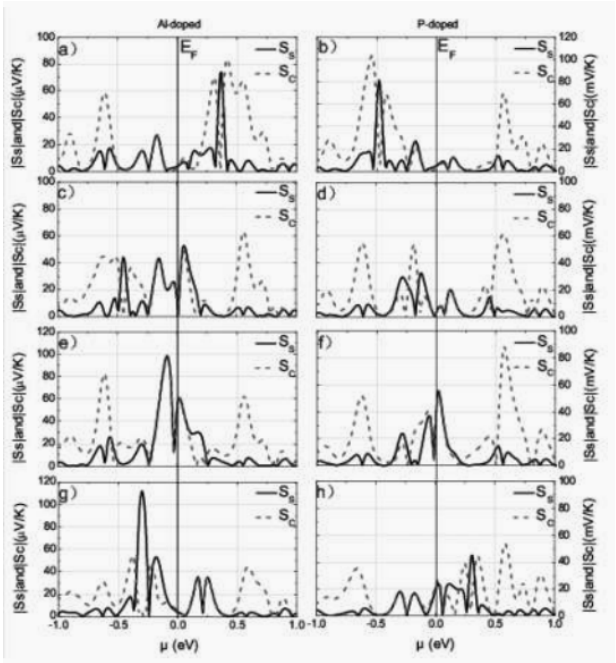

Figure 5. Ferromagnetic ZSiNRs (N = 6) doped with Al (left column) and P (right column) at zero bias with respect to chemical potential μ. The spin (charge) thermoelectric coefficient function $|S_s|(|S_c|)$. The black line and red line represent $|S_s|$ and $|S_c|$. The left and right columns represent $|S_s|(|S_c|)$ of ZSiNRs at different doping positions of Al (left) and P (right) respectively.

However, when the doping position is moved from position 2 to position 3, it can be seen from **Figures 4(e)** and **(f)** that in the Al-ZSiNRs (P-ZSiNRs) system μ = 0, $S_\uparrow(S_\downarrow)$ is greatly enhanced, but $S_\downarrow(S_\uparrow)$ is almost zero, resulting in $|S_s| \approx |S_c|$ (as shown in **Figures 5(e)** and **(f)**). When the doping position is moved to position 4, the spin related thermoelectric effect becomes relatively weak because the semi metallic property at the Fermi plane is transformed into metal property. Looking at **Figure 5(g)**, we find that for Al-ZSiNRs, at energy $\mu \approx -0.3$ eV, there is a high spin thermoelectric effect, while the corresponding charge thermoelectric coefficient is very small, al-

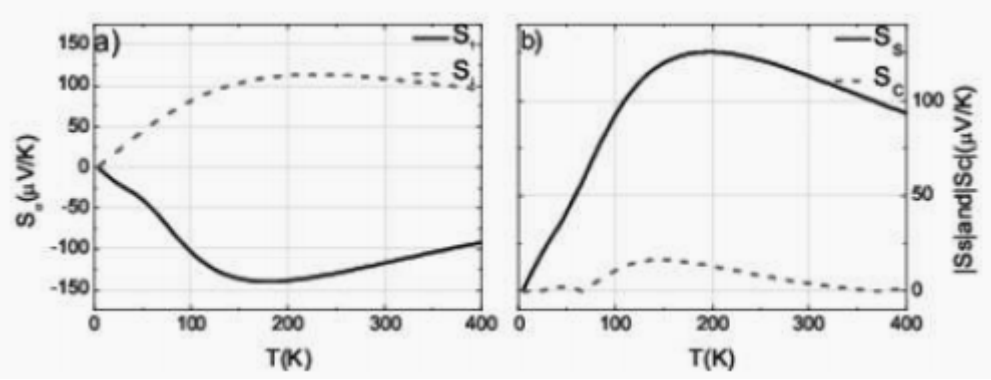

Figure 6. Chemical potential is fixed under zero bias voltage μ = –0.3 eV, when the doping position is 4, spin dependent thermoelectric coefficient S_σ of Al-ZSiNRs spin (charge) thermoelectric coefficient $|S_s|(|S_c|)$ versus temperature.

most zero. Therefore, we fix the chemical potential μ = –0.3 eV, and calculated the Al-ZSiNRs relation of S_σ and $|S_s|(|S_c|)$ with temperature T. The temperature range is taken as [0, 400 k] (as shown in **Figure 6**). As the temperature T changes from 0 to 400 K, the signs of $S_\uparrow$ and $S_\downarrow$ are opposite, and $|S_c|$ changes little in the whole temperature range, and its value is almost zero. Therefore, for the nano equipment based on ZSiNRs, we can obtain an almost ideal pure self-swirl generation device by doping Al atoms in specific parts.

4. Conclusion

We propose a spin thermoelectric device composed of doped silene nanoribbons (ZSiNRs). Here, the doping method of ZSiNRs is to replace the Si atom at the edge with Al and P atoms. We find that due to Al(P) doping, some spin up (down) quantum states appear near the Fermi level, which leads to the spin polarizability close to –100% (aluminum atom doping) and 100% (phosphorus atom doping). In addition, the thermoelectric coefficient of doped ZSiNRs, including spin dependent thermoelectric coefficient and spin (charge) thermoelectric coefficient, has been significantly strengthened. While Al atom doping at a specific position can obtain an ideal pure self-swirling thermoelectric device.

Conflict of interest

The authors declare that they have no conflict of interest.

Acknowledgements

This paper was supported by National Natural Science Foundation of China “Research on theory and application of molecular thermoelectric devices” (11247028).

References

1. Novoselov KS, Geim AK, Morozov SV, *et al.* Electric field effect in atomically thin carbon films. Science 2004; 306: 666–669.
2. Morishita T, Nishio K, Mikami M. Formation of single- and double-layer silicon in slit pores. Physical Review B, Condensed Matter 2008; 77: 081401(R).
3. Liu C, Feng W, Yao Y. Quantum spin hall effect in silicene and two-dimensional germanium. Physical Review Letters 2011; 107(7): 6802.
4. Liu C, Jiang H, Yao Y. Low-energy effective Hamiltonian involving spin-orbit coupling in silicene and two-dimensional Germanium and tin. Physical Review B 2011; 84(19): 5403.
5. Topsakal M, Ciraci S. Elastic and plastic deformation of graphene, silicene, and boron nitride honeycomb nanoribbons under uniaxial tension: A first-principles density-functional theory study. Physical Review B, Condensed Matter 2010; 81(2): 4107.
6. Padova PD, Quaresima C, Ottaviani C, *et al.* Evidence of graphene-like electronic signature in silicene nanoribbons. Applied Physics Letters 2010; 96(26): 1905.
7. Fang D, Zhang S, Xu H. Tuning the electronic and magnetic properties of zigzag silicene nanoribbons

by edge hydrogenation and doping. RSC Advances 2013; 3: 24075–24080.
8. Pan L, Liu H, Tan X, *et al.* Thermoelectric properties of armchair and zigzag silicene nanoribbons. Physical Chemistry Chemical Physics: PCCP 2012; 14: 13588–13593.
9. Zberecki K, Wierzbicki M, Barna J, *et al.* Thermoelectric effects in silicene nanoribbons. Physical Review B 2013; 88(11): 5404.
10. Uchida K, Takahashi S, Harii K, *et al.* Observation of the spin Seebeck effect. Nature 2008; 455(7214): 778–781.
11. Adachi H, Ohe J, Takahashi S, *et al.* Linear-response theory of spin Seebeck effect in ferromagnetic insulators. Physical Review B 2011; 83(9): 4410.
12. Jaworski CM, Myers RC, Johnston-Halperin E, *et al.* Giant spin Seebeck effect in a non-magnetic material. Nature 2012; 487(7406): 210–213.
13. Weiler M, Althammer M, Czeschka FD, *et al.* Local charge and spin currents in magnetothermal landscapes. Physics Review Letters 2012; 108(10): 6602.
14. Uchida K, Nonaka T, Kikkawa T. Longitudinal spin Seebeck effect in various garnet ferrites. Physical Review B, Condensed Matter 2013; 87(10): 4412.
15. Zeng M, Huang W, Liang G. Spin-dependent thermoelectric effects in graphene-based spin valves. Nanoscale 2013; 5(1): 200–208.
16. Liu Y, Yang X, Chi F, *et al.* A proposal for time-dependent pure-spin-current generators. Applied Physics Letters 2012; 101(21): 3109.
17. Liu Y, Wang X, Chi F. Non-magnetic doping induced a high spin-filter efficiency and large spin Seebeck effect in zigzag graphene nanoribbons. Journal of Materials Chemistry C 2013; 1(48): 8046–8051.
18. Chen A, Wang X, Vasiopoulous P, *et al.* Spin-dependent ballistic transport properties and electronic structures of pristine and edge-doped zigzag silicene nanoribbons: Large magnetoresistance. Physical Chemistry Chemical Physics 2014; 16(11): 5113–5118.
19. Kresse G, Hafner J. Ab-initio molecular dynamics for liquid metals. Physical Review B, Condensed Matter 1993; 47(1): 558–561.
20. Dubi Y, Ventra MD. Thermospin effects in a quantum dot connected to ferromagnetic leads. Physical Review B 2009; 79: 081302(R).